ACS OMEGA

http://pubs.acs.org/journal/acsodf

Article

Instantaneous Adsorption of Synthetic Dyes from an Aqueous Environment Using Kaolinite Nanotubes: Equilibrium and Thermodynamic Studies

Mostafa R. Abukhadra,* Merna Mostafa, Ahmed M. El-Sherbeeny,* Mohammed A. El-Meligy, and Ahmed Nadeem

Cite This: *ACS Omega* 2021, 6, 845−856

Read Online

ACCESS | Metrics & More | Article Recommendations | Supporting Information

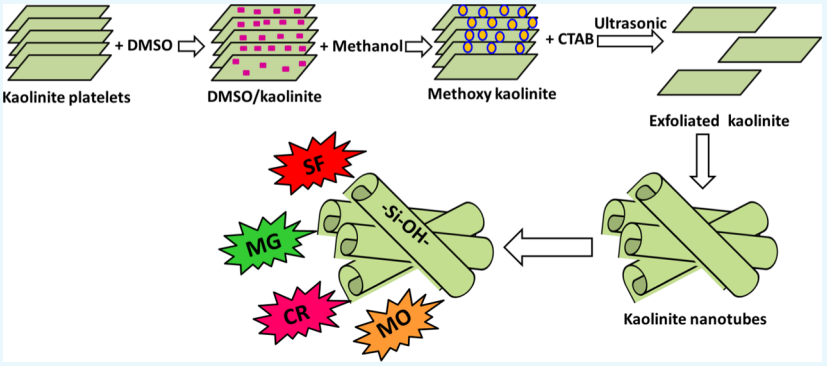

ABSTRACT: Innovative kaolinite nanotubes (KNTs) are synthesized utilizing a simple technique involving a sonication-induced exfoliation process, followed by chemical scrolling reactions. The KNTs as a material have high reactivity and promising surface area to be used in the purification of water from cationic dyes (safranin (SF) and malachite green (MG)) and anionic dyes (methyl orange (MO) and Congo red (CR)). The kinetic studies of the four dyes SF, MG, CR, and MO show an equilibration time interval of 240 min. The SF, MG, CR, and MO dyes' uptake reactions are in agreement with the kinetic behavior of the pseudo-first-order model and the equilibrium properties of the Langmuir model. Such modeling results, in addition to the Gaussian energies from the Dubinin−Radushkevich (D−R) model (SF (1.01 kJ/mol), MG (1.08 kJ/mol), CR (1.11 kJ/mol), and MO (1.65 kJ/mol)), hypothesize monolayer adsorption of the four dyes by physical reactions. The KNTs show theoretical q_{max} values of 431.6, 489.9, 626.2, and 675.5 (mg/g) for SF, MG, CR, and MO, respectively. The thermodynamic examination of SF, MG, CR, and MO adsorption reactions using KNTs verifies their adsorption by exothermic and spontaneous reactions. The KNT adsorbents achieve promising adsorption results in the presence of different coexisting ions and show significant recyclability properties. Therefore, the production of KNTs from kaolinite shows a strong effect on inducing the textural, physicochemical, and adsorption properties of clay layers as well as their affinity for different species of synthetic dyes.

1. INTRODUCTION

Extensive monitoring of various species of toxic inorganic, organic, suspended, and biological water pollutants is highly important for the safety of our contemporaneous world as they have direct negative and poisonous effects on freshwater resources, aquatic organisms, and plants.[1−3] Synthetic dyes are identified as one of the extensively detected organic contaminants in different water supplies. About 90% of the known synthetic dyes are classified as toxic and hazardous compounds that can cause eutrophication, perturbation of the aquatic ecosystem, and esthetic pollution in addition to their threats to human health.[4−6] Safranin (SF), malachite green (MG), methyl orange (MO), and Congo red (CR) dyes are very common types of dyes that are extensively used in several industrial and human activities.[7−9]

Safranin (SF) is a synthetic dye that is of basic type, and its existence in water supplies is recognized as the main reason for some negative health impacts such as respiratory tract irritation and skin irritation in addition to its role in causing injury to the conjunctiva as well as the cornea of the human eyes.[10,11] Also, malachite green (MG) is a common type of highly toxic synthetic dye that is used extensively in aquaculture, medical, and food industries.[4,12] Chromosomal fractures, mutagenesis,

Received: November 6, 2020
Accepted: December 11, 2020
Published: December 23, 2020

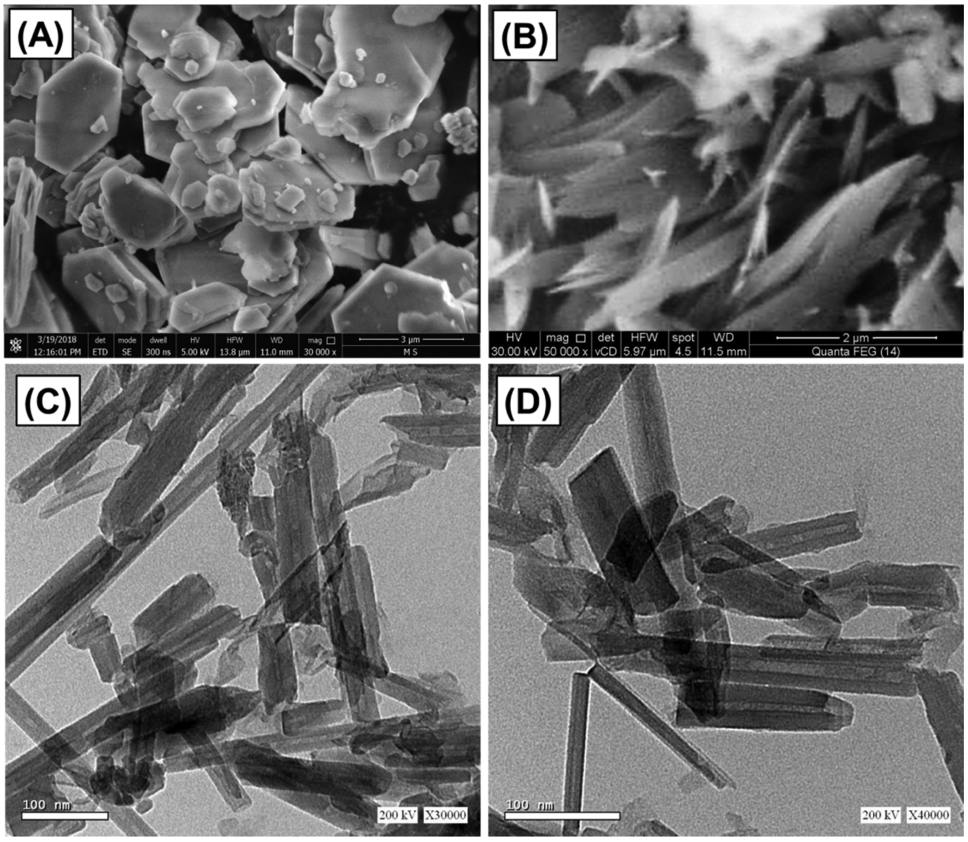

Figure 1. SEM images of the kaolinite mineral (A) and KNTs (B) and HRTEM images of the produced KNTs (C, D).

carcinogenesis, respiratory toxicity, and teratogenicity are the commonly detected health side effects of malachite green as water pollutants.[13,14] Such hazardous impacts have also been reported for the acidic Congo red (CR) dye, which is a highly soluble synthetic dye and is applied widely in cosmetic, plastic, and textile industries.[15,16] The presence of the Congo red dye in drinking water leads to significant toxic, carcinogenic, and mutagenic effects.[2,16,17] Methyl orange (MO) is another type of acidic synthetic dye that has a vital role in the textile as well as the printing industries.[5,18,19] The release of the MO dye at high concentrations has several dangerous effects as it is a toxic compound with carcinogenic and mutagenic properties.[19,20]

Development of promising decontamination techniques for such organic pollutants utilizing natural minerals and rocks was recommended as they are economic and easily available.[21] Also, there have been continuous scientific efforts from the environmental authorities and innovative researchers to produce novel forms of adsorbents that achieved promising capacities within small time intervals.[22] One-dimensional nanostructures like nanorods and nanotubes as well as clay-based nanomaterials were studied widely for the adsorption of different species of water contaminants because of their high surface area and high dispersion properties.[23,24]

Recently, synthetic kaolinite nanoscrolls or nanotubes (KNTs) were developed from natural kaolinite minerals and investigated as novel adsorbents for metal ions.[25] Kaolinite is a clay mineral with a 1:1 sheet structure and a hydrated aluminum silicate chemical structure.[14,26] It was reported that the chemical and morphological modifications of the kaolinite sheets have a strong influence on enhancing the surface reactivity, the adsorption capacity, and the surface area of kaolinite.[15,28] The scrolling process of the well-developed kaolinite layered units into different types of nanotubes was observed as one of the best structural and morphological modification techniques, which results in a semicrystalline product having promising physicochemical properties and a porous structure.[28] Therefore, the production of nanoscrolls or nanotubes from the kaolinite mineral will result in a promising adsorbent material with amazing adsorption properties, low production cost, simple preparation steps, and abundant natural resources for its precursor.

Unfortunately, there are no previous research studies that investigated the adsorption affinities and capacities of the KNT structure for organic pollutants, especially synthetic dyes, as well as the predicted adsorption mechanism. Therefore, this study aims to investigate the adsorption properties of synthetic kaolinite nanotubes (KNTs) as an effective and new adsorbent for different types of basic synthetic dyes (safranin dye and malachite green dye) and acidic synthetic dyes (methyl orange and Congo red dyes) and a potential product for large-scale applications. The study involves evaluation of the adsorption properties of KNTs considering the main variables of pH, contact time, dye concentrations, dosage, coexisting ions, and temperature. Additionally, the addressed dye adsorption systems are explained based on the scientific significance of their thermodynamic, equilibrium, and kinetic properties.

2. RESULTS AND DISCUSSION

2.1. Characterization of KNTs. The formation of KNTs was confirmed by both scanning electron microscopy (SEM) and high-resolution transmission electron microscopy (HRTEM) images (Figure 1). The pseudohexagonal flakes of the kaolinite mineral (Figure 1A) were converted strongly

https://dx.doi.org/10.1021/acsomega.0c05430
ACS Omega 2021, 6, 845−856

into scrolled or folded particles of tubular forms (Figure 1B). The deep investigation of the scrolled particles in the HRTEM images reflected their formation as nanotubes of cylindrical hollow forms with an internal diameter from 2 up to 20 nm (Figure 1C,D) as compared to the pure flaky nature of kaolinite (Figure S1). The length of produced KNTs ranged from nearly 50 to about 600 nm, and the outer diameters of these tubes were detected within a range from 10 up to 50 nm.

As we presented in our previous studies, the used kaolinite mineral was identified by its diffraction peaks at 12.33° (001), 20.8° ($\bar{1}$10), 24.87° (002), and 26.6° (111) that were related to its triclinic crystal system (Figure 2A.A). Dimethyl sulfoxide

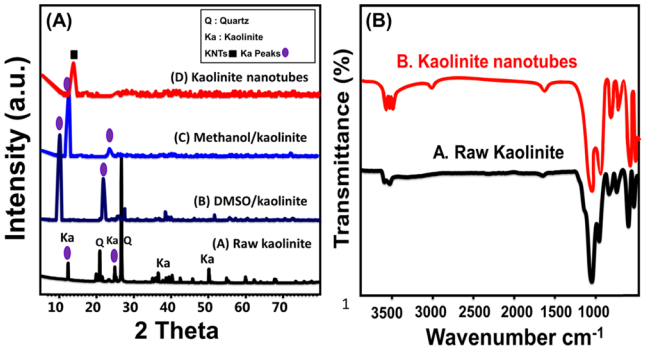

Figure 2. XRD patterns of the kaolinite mineral, DMSO/kaolinite, methoxy kaolinite, and KNTs (A) and the Fourier transform infrared (FT-IR) spectra of the kaolinite mineral and KNTs (B).

(DMSO)-intercalated kaolinite layers showed a reduction for most of the kaolinite peaks except the main peaks ((001) and (002)) that were observed as broad and deviated peaks (Figure 2A.B). The same two peaks were observed for methoxy kaolinite but with lower intensities than the observed peaks for DMSO/kaolinite (Figure 2A.C). After the complete formation of KNTs, the obtained pattern displays only one peak at nearly 10.6° that signifies the (001) plane of kaolinite scrolls (Figure 2A.D).[25]

Comparing the FT-IR spectrum of kaolinite with the one obtained for KNTs reflected no obvious changes in the chemical composition (Figure 2B). The spectrum of the kaolinite mineral demonstrated the existence of Si−O, Si−O−Al groups, Si−O−Si, OH bending, Al−OH, and Si−OH groups considering their identification bands at 456, 680, 1020, 1641, 912, 3500.2, and 3689.4 cm^{-1}, respectively (Figure 2B.A).[15] The same bands were observed for KNTs but at shifted positions, which suggested distortion of the basic kaolinite units during the conversion processes (Figure 2B.B). Also, the expected binding of the intercalated organic compounds with the siloxane groups or the basal oxygen has substantial impact on the structural units of KNTs.[28]

As for the texture of KNTs, the change of the isotherm curve from type II for the kaolinite mineral to type IV with an H3 hysteresis loop for KNTs reflected changes in the morphology from macroporous plates to nanoporous materials in which the pores were of tubular or cylindrical forms[25] (Figure S2). Therefore, the surface area increased from 10 m^2/g for the kaolinite mineral to 105 m^2/g for KNTs. Moreover, the total porosity increased significantly from 0.052 cm^3/g for the kaolinite mineral to 0.51 cm^3/g for KNTs. The average pore diameter of the produced KNTs was 12 nm, and hence they could be regarded as having a mesoporous structure. Also, the transformation of the flaky sheets of kaolinite into nanotubes had a slight effect on the ion-exchange properties. The ion-exchange capacity slightly increased from 3 mequiv/100 g to 5.2 mequiv/100 g after the production of KNTs. This is in agreement with the expected distortion in both the silicon tetrahedrons and the aluminum octahedrons of kaolinite.

2.2. Influence of Process Variables on Adsorption.

2.2.1. Influence of pH on Adsorption. The pH value of the polluted water has a controlling effect on the ionization states of the dye molecules as well as the surficial charges of the solid adsorbents.[29] The experiments considering the influence of pH as the essential variable were carried out for a wide range from highly acidic pH 2 to alkaline pH 10. Moreover, the other studied variables were considered at selected experimental values of 500 mL as the treated volume, 120 min as the tested contact time, 0.2 g/L as the KNT solid dosage, adjusted 100 mg/L as the tested concentration of the four dyes, and 25 °C as the operating temperature. However, the affinity of KNTs for SF and MG dyes significantly increased on performing the tests under alkaline conditions, and their uptake capacity for CR and MO dyes declined strongly under such basic environments (Figure 3). These different adsorption trends

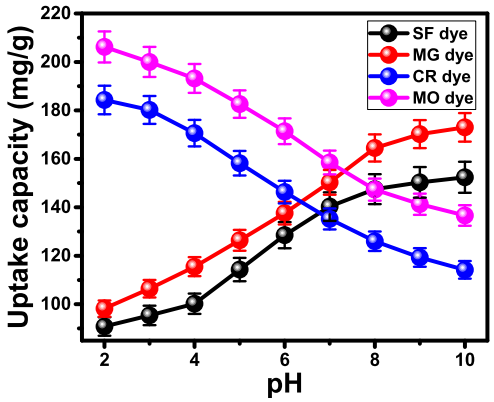

Figure 3. Effect of solution pH values on the uptake capacities of KNTs for SF, MG, CR, and MO dyes.

are related to the ionization properties of the dyes as the SF and MG dyes are of cationic type, while the CR and MO dyes are of anionic type. Therefore, the deprotonated sites of KNTs that are negatively charged receptors at such basic environments have highly attractive properties for cationic SF and MG dyes (positively charged molecules) and strong repulsive properties for anionic CR and MO dyes (negatively charged molecules).[30] Moreover, the reported dipolar properties of CR as cationic molecules under acidic environments (pH < 5.5) and as anionic molecules at pH values higher than 5.5 greatly affected the adsorption behaviors of CR molecules.[31] The greatest uptake capacities for SF (152.4 mg/g) and MG (173 mg/g) were achieved at pH 10. On the other hand, the highest uptake capacities of CR (184.3 mg/g) and MO (206.2 mg/g) dyes were observed at pH 2 (Figure 3). The previously mentioned results and the related explanation were supported by the detected pH value of zero point charge ($pH_{(zpc)}$) considering the measured ζ potential values. The measured $pH_{(zpc)}$ value of KNTs is 6.73, and this value is close to that obtained for raw kaolinite (pH 6.54). The value of the $pH_{(zpc)}$ reflected the enrichment of the KNT surface with the negative charges during the adsorption of the four dyes at pH values

https://dx.doi.org/10.1021/acsomega.0c05430
ACS Omega 2021, 6, 845−856

higher than these values. This value is close to the obtained value for kaolinite (pH 6.54).

2.2.2. Influence of Contact Time on Adsorption. The uptake behaviors for SF, MG, CR, and MO dyes by KNTs were followed from 30 up to 600 min. The other inspected variables were considered at selected experimental values of 500 mL as the treated volume, 0.2 g/L as the KNT solid dosage, 100 mg/L as the tested concentration of the four dyes, and 25 °C as the operating temperature. The adsorption pH values were selected to be 10 for SF and MG cationic dyes and 2 for CR and MO anionic dyes.

The observed SF, MG, CR, and MO adsorption curves are of segmental shapes and different slopes, which suggested strong variations in the dye uptake rates (Figure 4). The

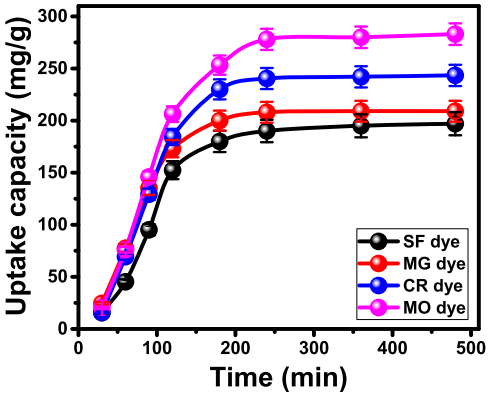

Figure 4. Uptake behaviors of SF, MG, CR, and MO dyes as a function of the contact time using KNTs.

observed segments during the initial stages of the curves for both the cationic and anionic dyes are of steep slopes (Figure 4). This proves an immediate increase in the adsorbed dye molecules with the initiation of the KNT-based adsorption reactions. This is followed by noticeable segments of small slopes or nearly plateau forms, signifying limited or nearly fixed variations in the dye adsorption rates. These segments are commonly identified as the saturation or the equilibration segments (Figure 4). The reported decrease in the KNT uptake rates for the dyes on increasing the studied contact time depends on the availability of the effective uptake sites.[30] The receptor sites of KNTs were highly available during the initiation of the reaction, which caused abrupt capturing of the dye molecules. After a certain time, the receptors became mostly occupied by the dye molecules, making the KNTs' capacity restricted to the remaining sites on the surface of KNTs.[22] The equilibrium time was identified as 240 min for SF, MG, CR, and MO dyes with equilibration capacities of 197, 209, 243.4, and 283 mg/g, respectively (Figure 4).

2.2.3. Influence of Dye Concentrations on Adsorption. Evaluation of the behavior of KNTs during the uptake of different concentrations of SF, MG, CR, and MO dyes (50–400 mg/L) is essential to determine its maximum capacity and its equilibrium properties.[32] The other studied variables were considered at selected experimental values of 500 mL as the treated volume, 0.2 g/L as the KNT solid dosage, 480 min as the reported equilibrium time, and 25 °C as the operating temperature. The adsorption pH was selected to be 10 for SF and MG cationic dyes and 2 for CR and MO anionic dyes. The quantities of the adsorbed anionic as well as cationic dyes by KNTs increased strongly on testing high concentrations of the four dyes (Figure S3). The intensification of the driving forces of the dye molecules at the highest concentrations supports the extensive interactions between their ions and the effective receptors of KNTs.[28,33] This can be detected for SF, MG, CR, and MO until tested concentrations of 300, 250, 300, and 200 mg/L, respectively, which are the equilibrium concentrations of the studied systems (Figure S3). Such concentrations resulted in complete or partial saturation of the sites of KNTs by the dye molecules, at which the material could attain its maximum capacity. The experimentally detected maximum capacities for SF, MG, CR, and MO dyes are 427.6, 464.4, 586.5, and 639.2 mg/g, respectively (Figure S3).

2.2.4. Influence of KNT Dosages on Adsorption. The predicted influence of KNT quantities on the removal of SF, MG, CR, and MO dyes was studied experimentally from about 0.2 to 1 g/L. The other studied variables were considered at selected experimental values of 500 mL as the treated volume, 480 min as the reported equilibrium time, 100 mg/L as the tested concentration of the four dyes, and 25 °C as the operating temperature. The adsorption pH was selected to be 10 for SF and MG cationic dyes and 2 for CR and MO anionic dyes. Figure 5 verifies significant and positive effects of KNT

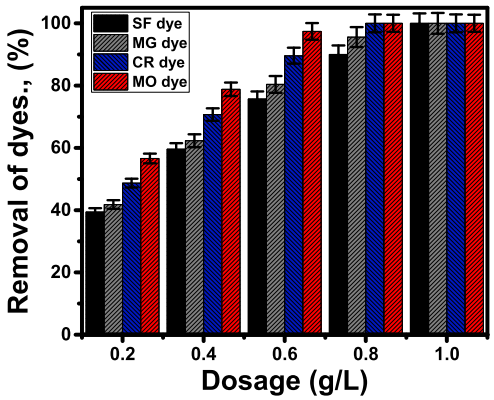

Figure 5. Removal percentages of SF, MG, CR, and MO dyes using different dosages of KNTs.

dosage on increasing the removal efficiency of SF, MG, CR, and MO dyes. This was explained to be associated with the enrichment of the dye solutions in the active sites of KNTs.[4] The adsorption percentage of the SF dye was enhanced from 39.5 up to 100% with the increase of the KNT dosage from 0.2 up to 1 g/L. For the MG cationic dye, the attained percentage using 0.2 g/L KNTs (41.8%) was augmented to 100% after using 1 g/L (Figure 5). Also, the removal of CR and MO anionic dyes significantly increased by the used KNT dosage as the examined concentrations (100 mg/L) were totally removed using about 0.8 g/L KNTs (Figure 5).

2.3. Kinetic and Equilibrium Studies. *2.3.1. Kinetic Modeling.* The kinetic study of SF, MG, CR, and MO uptake reactions by KNTs was accomplished by the mathematical fitting process of the experimental results with the formula of the intraparticle-diffusion model. Additionally, the pseudo-first-order, the pseudo-second-order, and the Elovich models were adopted in this study. The descriptive equations of these models, which were used in the fitting of SF, MG, CR, and MO data, are listed in Table S1. The SF, MG, CR, and MO intraparticle-diffusion curves have three obvious segments without intersection with the source points (Figure 6A). These segments verified the existence of different types of dye

https://dx.doi.org/10.1021/acsomega.0c05430
ACS Omega 2021, 6, 845−856

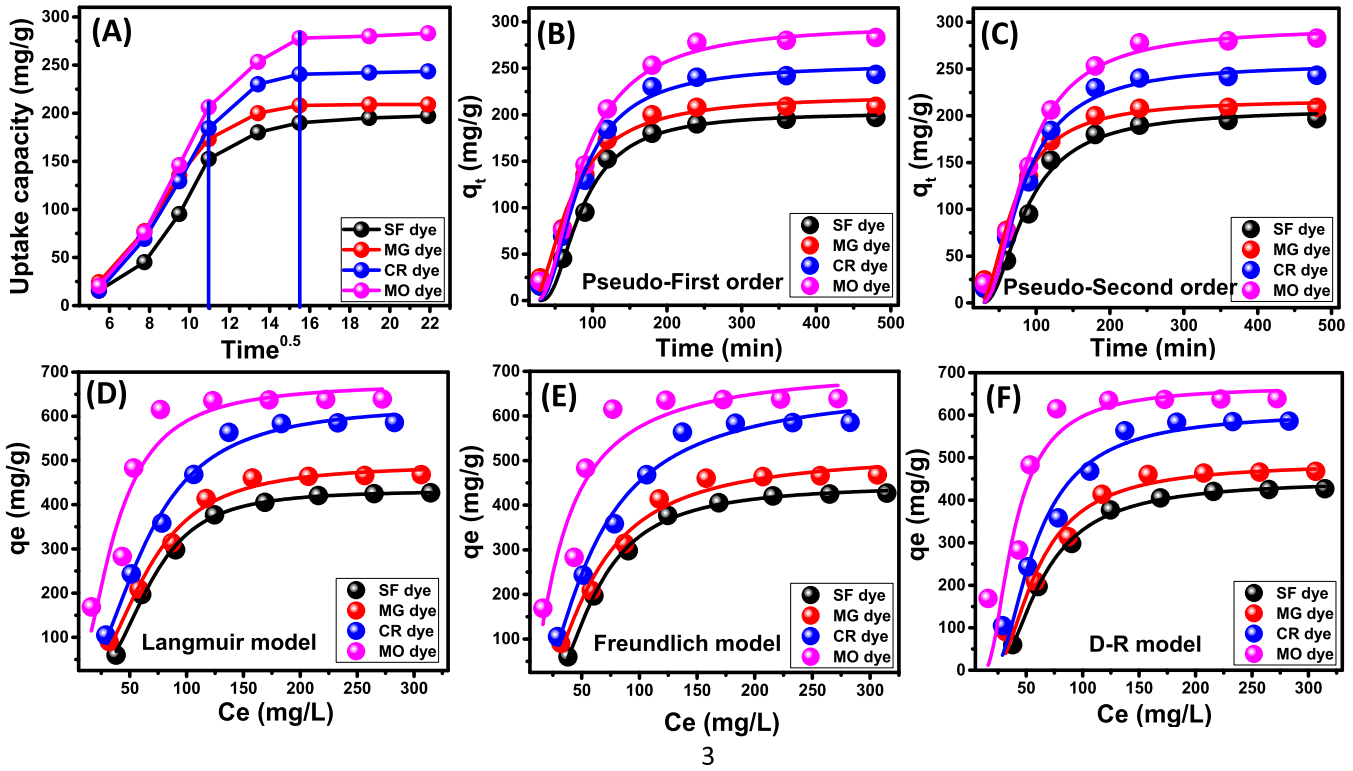

3

Figure 6. Fitting of the dye adsorption data with (I) intraparticle diffusion model, (B) pseudo-first-order kinetic model, (C) pseudo-second-order kinetic model, (D) Langmuir isotherm model, (E) Freundlich isotherm model, and (F) Dubinin−Radushkevich isotherm model.

Table 1. Theoretical Parameters for the Investigated Kinetic and Equilibrium models

kinetic models					
model	parameters	SF	MG	CR	MO
pseudo-first-order	K_1 (min^{-1})	4.9×10^{-7}	7.47×10^{-5}	2.72×10^{-6}	4.49×10^{-6}
	$q_{e(Cal)}$ (mg/g)	202	217	251.7	294.3
	R^2	0.98	0.98	0.99	0.99
	χ^2	2.12	1.86	1.12	0.87
pseudo-second-order	k_2 (g/(mg min))	2.49	1.95	2.26	2.09
	$q_{e(Cal)}$ (mg/g)	207	221.4	254.2	297
	R^2	0.98	0.98	0.98	0.98
	χ^2	2.7	2.54	1.45	1.22
Elovich	β (g/mg)	0.013	0.014	0.011	0.01
	α (mg/(g min))	3.23	4.49	4.2	4.72
	R^2	0.88	0.86	0.89	0.91
	χ^2	5.8	6.6	5.3	4.2
isotherm models					
model	parameters	SF	MG	CR	MO
Langmuir	q_{max} (mg/g)	431.6	489.9	626.2	675.5
	b (L/mg)	3.7×10^{-6}	4.07×10^{-5}	1.02×10^{-4}	9.3×10^{-4}
	R^2	0.99	0.98	0.98	0.90
	χ^2	0.87	2.14	2.23	3.6
	R_L	0.99−0.998	0.98−0.997	0.96−0.99	0.73−0.95
Freundlich	$1/n$	0.45	0.57	0.63	0.71
	k_F (mg/g)	182	234.5	128.8	30.7
	R^2	0.99	0.97	0.97	0.87
	χ^2	2.3	4.7	4.36	5.7
D−R model	β (mol^2/kJ^2)	0.496	0.43	0.403	0.183
	q_m (mg/g)	446	486.9	607.4	667.8
	R^2	0.99	0.96	0.95	0.84
	χ^2	4.6	6.23	6.8	7.3
	E (kJ/mol)	1.01	1.08	1.11	1.65

https://dx.doi.org/10.1021/acsomega.0c05430
ACS Omega 2021, 6, 845−856

adsorption mechanisms that were not restricted only to the diffusion reaction of the dye molecules toward the receptors of KNTs.[21] The first segment was the dominant one in the four curves and hypothesized uptake of SF, MG, CR, and MO dyes essentially by the exterior receptors of KNTs[27] (Figure 6A). This showed the uptake of most of the dissolved dye molecules (SF, MG, CR, and MO) by this mechanism.

This was followed by another segment that covered a significant period during the uptake of SF, MG, CR, and MO dyes (Figure 6A). This segment emphasized diminution of the external adsorption mechanism as all of the external receptors of KNTs were consumed by the molecules of the four dyes. Additionally, this segment verified the dominance of the layered adsorption processes as the essential mechanism and their considerable role during the uptake of SF, MG, CR, and MO dyes by KNTs at the intermediate stages of the reactions.[25,34] By the end of this segment, another new segment was detected in the curves of SF, MG, CR, and MO dyes that appeared to be of negligible effect (Figure 6A). This segment was detected basically after the saturation of all of the external and internal receptors of KNTs by the dye molecules. The observation of this segment establishes the uptake of SF, MG, CR, and MO as thick coating layers for the KNT fractions and might be formed by inter-ionic attraction or by different types of molecular association processes.[34]

The χ^2 values as well as the values of correlation coefficient (R^2) were used to study the fitting degree of adsorption data of SF, MG, CR, and MO dyes with the other three kinetic models (Figure 6B,C). Although two models (pseudo-first- and pseudo-second-order models (Figure 6B,C)) had high correlation coefficients for the four dyes, the χ^2 values suggested better agreement with the first-order supposition than the second-order supposition (Table 1). Such fitting results declared the adsorption of the dyes by physical processes which will be supported by further equilibrium studies.[35] The estimated values of the experimental SF (197 mg/g), MG (209 mg/g), CR (243.4 mg/g), and MO (283 mg/g) uptake capacities (q_e) close to the theoretical values from the pseud-first-order model (202 mg/g (SF), 217 mg/g (MG), 251.7 mg/g (CR), and 294.3 mg/g (MO)) support the fitting results (Table 1).

The significant fitness of the adsorption data of the four dyes with the second-order supposition demonstrated the existence of some supporting mechanisms that have more chemical characteristics such as the surface complexation reactions, electron sharing reactions, and electron exchange reactions.[36] This was confirmed by the considerable agreement between the dye adsorption data and the Elovich kinetic model, which also reflected the energetic heterogeneous surface of KNTs during the uptake of SF, MG, CR, and MO dyes[37] (Figure S4).

2.3.2. Isotherm Modeling. The equilibrium behaviors of SF, MG, CR, and MO adsorption reactions using KNT adsorbents were followed considering the extent of agreement with the hypothesis of the theoretical Langmuir and Freundlich models in addition to the Dubinin–Radushkevich (D–R) model (Table S1). The correlation coefficients (R^2), as well as the χ^2 parameters of the fitting processes, are presented in Table 1. The uptake of the cationic dyes (SF and MG) and the anionic dyes (CR and MO) followed the presumption of the Langmuir (Figure 6D) rather than the Freundlich model (Figure 6E). This hypothesized the existence of the adsorbed SF, MG, CR, and MO dyes in monolayer forms and verified their uptake by different types of homogeneous active sites on the reactive surface of KNTs.[25] Moreover, the adsorption of SF, MG, CR, and MO dyes occurred by favorable reactions as estimated from their R_L parameters (Table 1). The predicted q_{max} values of SF, MG, CR, and MO dyes were calculated from the Langmuir fitting process and were 431.6, 489.9, 626.2, and 675.5 mg/g, respectively.

The assessment of the D–R isotherm model was performed using values of its theoretical parameters for understanding the nature of SF, MG, CR, and MO adsorption reactions as well as their maximum adsorption capacities (Figure 6F). The Gaussian energies (SF-1.01, MG-1.08, CR-1.11, and MO-1.65 (kJ/mol)) were calculated from the excellent fitting with the D–R model, and the reported values were related essentially to physical adsorption reactions (less than 8 kJ/mol)[21] (Figure 6F and Table 1). Additionally, the expected q_{max} values of SF, MG, CR, and MO as fitting parameters for the model were 446, 486.9, 607.4, and 667.8 mg/g, respectively.

2.4. Thermodynamics. The thermodynamics of SF, MG, CR, and MO adsorption reactions using the prepared KNT adsorbent were followed within an experimentally studied temperature range from 25 °C as the starting value to 45 °C as the upper value. The other studied variables were considered at selected experimental values of 500 mL as the treated volume, 0.2 g/L as the KNT solid dosage, 100 mg/L as the tested concentration of the four dyes, and 480 min as the contact time. The adsorption pH was selected to be 10 for SF and MG cationic dyes and 2 for CR and MO anionic dyes. The essential descriptive parameters of the thermodynamic properties ($\Delta H°$ (enthalpy), $\Delta S°$ (entropy), and $\Delta G°$ (Gibbs free energy)) are presented in Table 2. Both $\Delta H°$ and $\Delta S°$ values were determined based on the commonly used linear fitting process between the experimental data and van't Hoff equation (eq 1) (Figure S5). The value of the incorporated Langmuir constant (K_c) in eq 1 was determined from eq 2 where the K_d constant is the ratio of the dye uptake capacities to their equilibrium concentrations.[38] The $\Delta G°$ values as theoretical parameters were calculated from eq 3 directly.[25]

Table 2. Thermodynamic Parameters for the Uptake of SF, MG, CR, and MO Dyes by KNTs

parameters	temperature	SF	MG	CR	MO
$\Delta G°$ (kJ/mol)	298.15	−12.88	−13.12	−13.81	−14.60
	303.15	−12.95	−13.19	−13.92	−14.65
	308.15	−12.95	−13.25	−14.00	−14.67
	313.15	−12.88	−13.23	−14.12	−14.75
	318.15	−12.73	−13.18	−14.23	−14.87
	323.15	−12.64	−13.19	−14.36	−14.99
$\Delta H°$ (kJ/mol)		−16.15	−12.73	−7.45	−10.09
$\Delta S°$ (J/(K mol))		−10.67	1.48	21.33	14.99

$$\ln(K_c) = \frac{\Delta S°}{R} - \frac{\Delta H°}{RT} \quad (1)$$

$$K_c = K_d \times 55.5 \quad (2)$$

$$\Delta G° = -RT \ln K_c \quad (3)$$

The negative signs that were reported for the enthalpy values of the cationic dyes (SF (−16.15 kJ/mol) and MG (−12.73 kJ/mol)) as well as the anionic dyes (CR (−7.45 kJ/mol) and MO (−10.09 kJ/mol)) verified their exothermic adsorption by

https://dx.doi.org/10.1021/acsomega.0c05430
ACS Omega 2021, 6, 845–856

KNTs (Table 2). Moreover, the calculated entropy values with a negative sign for the SF dye and with positive signs for MG, CR, and MO dyes verified changes in randomness properties at the interface between KNTs and the tested dyes (Table 2). While the randomness properties of SF uptake reaction decreased with the temperature, the randomness of MG, CR, and MO uptake reactions increased observably with the temperature (Table 2).[21] The calculated free energies of SF, MG, CR, and MO adsorption reactions were negative values at all of the studied temperatures (Table 2). These negative values revealed spontaneous, feasible, and favorable dye uptake reactions in the presence of KNTs as the adsorbent.[21] The entropy and free energy values for the SF, MG, CR, and MO adsorption reactions were within the suggested range for the physisorption reactions, which strongly matched the results of the previously investigated kinetic and isotherm models.[29]

2.5. Recyclability. The suitability of KNTs to be recycled several times for the adsorption of the cationic and anionic dyes was assessed for five runs as a vital factor deciding the commercial value of the product. The regeneration of the KNT particles involved washing of KNTs with NaOH aqueous solution (0.2 M) at an adjusted temperature of 50 °C under continuous shaking for 3 h using an orbital shaker in a hot water bath for the samples that were used in the uptake of anionic dyes. The samples that were applied in the adsorption of cationic dyes were washed with dilute HCl acid (10%) for 60 min. Then, the solid KNT particles were isolated and washed again extensively using distilled water, and this was repeated for three cycles and each cycle was for 10 min. Finally, the washed KNT fractions were dried at 85 °C for 12 h and used in the next recyclability cycle. The accomplished adsorption recyclability experiments were conducted at the pre-identified best uptake conditions (500 mL as the treated volume, 480 min as the reported equilibrium time, 100 mg/L as the tested concentration of the four dyes, 1 g/L as the incorporated KNT solid dosage, and 25 °C as the operating temperature). The adsorption pH was selected to be 10 for SF and MG cationic dyes and 2 for CR and MO anionic dyes.

The obtained data for the KNT recyclability tests proved the high efficiency of KNTs in the adsorption of the four dyes for the addressed five runs considering the studied concentration (100 mg/L) (Figure S6). The KNTs as the adsorbent showed removal percentages for the SF dye higher than 97.5% for three recyclability cycles, higher than 94.4% for four recyclability cycles, and higher than 91% for the addressed five recyclability cycles (Figure S6). Also, MG removal percentages higher than 99% for two cycles, higher than 98.3% for four cycles, and higher than 93.5% for five cycles were obtained (Figure S6). For the CR dye, the recyclability studies emphasized removal percentages higher than 98.6% for three cycles and higher than 95% for five cycles (Figure S6). For the MO dye, removal percentages higher than 99% for three cycles, higher than 98.4% for four cycles, and higher than 96.5% for all of the studied five cycles were documented (Figure S6). The efficiency of KNTs for the adsorption of SF, MG, CR, and MO dyes showed a decrease with increasing number of recyclability tests. The continuous occupation of the main receptors by the dyes molecules and the expected binding between the siloxane groups and the dyes molecules caused a reduction in the availability of such sites and in turn the efficiency of KNTs.

2.6. Influence of Coexisting Ions. The role of coexisting anions together with their activity as competitive ions for SF, MG, CR, and MO dye molecules during their uptake by KNTs was studied using four types of commonly detected water pollutants (PO_4^{3-}, NH_4^+, Pb^{2+}, and Zn^{2+}). The performed experiments were assessed at the pre-identified best uptake conditions (500 mL as the treated volume, 480 min as the reported equilibrium time, 100 mg/L as the tested concentration of the four dyes, 1 g/L as the incorporated KNT solid dosage, and 25 °C as the operating temperature).

For the SF dye, the adsorption percentages dropped to 78.3, 86.4, 42.6, and 44.7% in the presence of PO_4^{3-}, NH_4^+, Pb^{2+}, and Zn^{2+} as coexisting ions, respectively (Figure 7). For the MG dye, the incorporation of PO_4^{3-}, NH_4^+, Pb^{2+}, and Zn^{2+} as competitive ions reduced the adsorption percentages to 82.6, 89.4, 47.2, and 53.6%, respectively (Figure 7). For the CR dye, its removal efficiency was also affected significantly by the existence of the selected competitive ions. The CR removal values reduced to 61.7, 90.4, 57, and 51.2% by the coexistence of PO_4^{3-}, NH_4^+, Zn^{2+}, and Pb^{2+}, respectively (Figure 7). Even for the removal of the anionic MO dye, the values reduced to 83.5, 92.6, 70.3, and 65.6% for the same coexisting ions of PO_4^{3-}, NH_4^+, Zn^{2+}, and Pb^{2+}, respectively (Figure 7). Generally, the presented results reflected a strong negative effect of the heavy metal ions on the affinity of KNTs for the SF and Mg dyes. Also, the chemical ions of phosphate and ammonium show considerable effect on the adsorption of these basic dyes. For the anionic dyes (CR and MO), the studied coexisting ions have significant impact on the affinity of KNTs for their molecules, but KNTs show a higher affinity for them in the presence of all of the studied competitive ions. The decrease in the affinity of KNTs for the dyes in the presence of coexisting ions was previously related to their competitive effect with dye molecules on the free active sites in addition to the predicted compensation of the solid charge by the ions.[39] Based on previously reported results, the KNT particles exhibit higher efficiency in the purification of water from the cationic and anionic dyes even in the presence of other species of water pollutants. This qualifies KNTs to be incorporated effectively in remediation techniques.

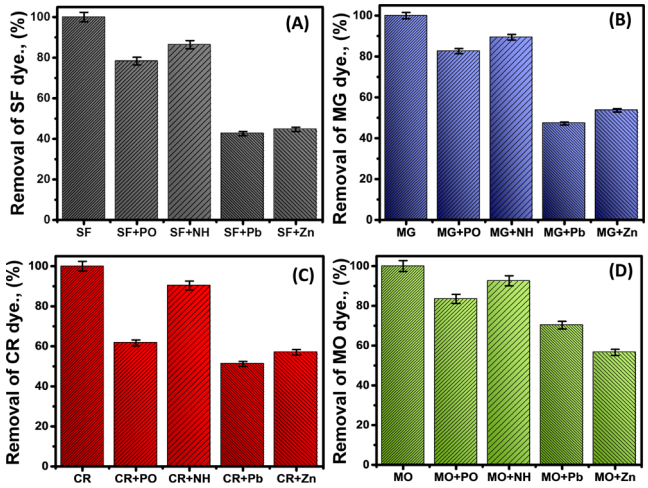

Figure 7. Effect of different coexisting (phosphate (PO), ammonium (NH), Pb^{2+} ions (Pb), and Zn^{2+} ions (Zn)) ions on the uptake of SF (A), MG (B), CR (C), and MO (D) dyes using KNTs.

2.7. Adsorption Mechanism. KNTs as a modified clay nanostructure are a highly active scrolled tetrahedron and octahedron sheets of kaolinite mineral. Such scrolled layered

https://dx.doi.org/10.1021/acsomega.0c05430
ACS Omega 2021, 6, 845−856

Table 3. Comparison between the Adsorption Capacities of KNTs and Other Natural and Synthetic Adsorbents for SF, MG, CR, and MO Dyes

cationic dyes			anionic dyes		
adsorbent	q_{max} (mg/g)	reference	adsorbent	q_{max} (mg/g)	reference
Safranin Dye			Congo Red Dye		
Ppy NF/Zn−Fe LDH	63.4	22	serpentine	93.45	33
glass-MCM-48	62.5	46	phosphate/kaolinite	149.25	14
activated carbon	576	47	chitosan/montmorillonite	290	16
MCM-41	68.8	48	willow leaf AlOOH	420	64
MgO-FLG-FE	201.1	49	Na montmorillonite	58.21	15
araphene oxide/chitosan	425	50	HDTMA/clinoptilolite	200	65
N/porous graphite	20.66	30	ZnO−AlOOH	524	64
fume-MCM-48	57.47	46	Mg−Al LDH	584.6	66
clinoptilolite	42.9	10	Ni/Co-LDH	909.2	67
ferruginous kaolinite	59.3	51	CTAB−H_2SO_4/celery residue	526	68
magnetic clay	18.48	52	hierarchical ZnO	334	64
raw kaolinite	14.37	this study	NiO−Al_2O_3	357	69
KNTs	431.6	this study	γ-Al_2O_3	416	70
Malachite Green Dye			bentonite/zeolite-NaP	46.29	71
Pinus roxburghii cone	250	13	$NiCo_2O_4$	366	72
activated carbon	395	5	NiO	534	73
MBCNF/GOPA	270.27	53	Raw kaolinite	40.6	this study
chitosan/polyacrylic acid/bentonite	454.55	54	KNTs	626.2	this study
Artocarpus odoratissimus leaves	422	55	Methyl Orange Dye		
CMC-g-P(AAm)	158.1	56	chitosan/bentonite	136.8	74
CMC-g-P(AAm)/MMT	172.4	56	CH/poly(vinyl alcohol)/zeolite	153	75
nanochitosan-STP	317	57	pHEMA-chitosan-MWCNTs	306	76
graphene oxide/lignin aerogels	113.5	11	functionalized CNTs/TiO_2	42.85	77
Fe_3O_4/PT/GO	560.58	58	functionalized CNTs	310	78
biochar/nZVI	515.77	59	zeolite NaA/CuO	79.42	79
mesoporous carbon	476.1	60	NiFe-LDH	169	80
reduced graphene oxide	576.2	61	acid-salt/CoAl LDH	827.4	81
activated carbon	210.1	62	h-MoS_2	41.5	19
carbon/Zn−Al-LDH	126.58	63	3D l PbS/ZnO	159	17
raw kaolinite	63.4	this study	raw kaolinite	11.5	this study
KNTs	489.9	this study	KNTs	675.5	this study

units are characterized by highly exposed and dominant siloxane groups (Al−OH and Si−OH).[40] The siloxane groups were reported as very active groups that have strong reactivity to form a complex with different species of dissolved chemical ions in addition to their role in the capturing of such ions by different types of electrostatic interactions.[40] The obtained FT-IR spectra of the incorporated KNTs for the adsorption of SF, MG, CR, and MO showed a strong reduction for the well-known bands of Al−OH and Si−OH (Figure S7). Such observations might be related to their predicted consumption during the adsorption of the four dye molecules. This emphasizes their role as essential sites during the electrostatic attraction of the charged dye molecules. The observation of several bands related to the chemical groups of the studied dyes indicated their effective role in the complexation processes during the capturing of SF, MG, CR, and MO molecules by KNTs (Figure S7). The reported groups of SF molecules are −NH (3460 cm^{-1}) and aromatic-N groups (1334 cm^{-1}), C═C (1603 cm^{-1}), and C−H (1422 cm^{-1}).[41] The reported chemical groups of MG are C−H (2960 cm^{-1}), C═C (1573.4 cm^{-1}), and C−N (1324 cm^{-1}).[42] The identified groups of CR are −CH2 (2934 cm^{-1}), N═N (1580 cm^{-1}), and C−N (1410 cm^{-1}). The identified groups of the MO dye are C−H (stretching, 2973 cm^{-1}), C═C (vibration, 1584 cm^{-1}), and N═N (1534 cm^{-1}).[43] Previous results verified the occurrence of a strong interaction between the siloxane groups (OH-bearing groups) and the ions of the four dyes forming new hydrogen bonds.[41,44]

Therefore, the adsorption mechanism of SF, MG, CR, and MO molecules by KNTs involved two essential mechanisms. The first mechanism was related to the chemical complexation of the exposed Al−OH and Si−OH groups or the basal oxygen of the structural units of KNTs and the ions of the studied dyes by different types of hydrogen bonding.[45] The second mechanism was related to different types of electrostatic attraction between the charged dye ions and the charged structural units of KNTs.[45] Other studies verified the effective role in the predicted intercalation of the layered units by the organic pollutants, which was supported by the presence of KNTs as multilayer scrolls of kaolinite.[44]

2.8. Comparison Study. The achieved SF, MG, CR, and MO uptake capacities by KNTs compared well with other highly effective adsorbents reported in the literature (Table 3). The synthetic KNTs as an adsorbent for both the cationic and anionic dyes show higher efficiency than most of the listed adsorbents in the table. The KNTs as a modified form of kaolinite appears to be more promising than several types of clay minerals such as kaolinite, bentonite, serpentinite, and halloysite either in their pure phase or their modified forms. The presented results reflected obvious enhancement in the

https://dx.doi.org/10.1021/acsomega.0c05430
ACS Omega 2021, 6, 845−856

affinity of the kaolinite layers after their scrolling process into nanotubes as compared to the normal flaky layers. This is related mainly to the increase in the reactivity and the surface area of KNTs as compared to raw kaolinite. Also, it showed higher capacities than several synthetic adsorbents including CNT-based adsorbents, LDH-based adsorbents, some biogenic adsorbents, some polymers, and some metal oxide-based adsorbents (Table 3).

3. CONCLUSIONS

Kaolinite nanotubes (KNTs) were produced and used in the purification of water from cationic dyes (safranin dye (SF) and malachite green dye (MG)) and anionic dyes (methyl orange dye (MO) and Congo red dye (CR)). The product exhibited theoretical q_{max} values of 431.6, 489.9, 626.2, and 675.5 mg/g for SF, MG, CR, and MO, respectively. The SF, MG, CR, and MO dye uptake reactions fitted excellently with the kinetic behavior of the pseudo-first-order (R^2 > 0.9) model and equilibrium behavior of the Langmuir model (R^2 > 0.9). The equilibrium results, the thermodynamic parameters, and the values of Gaussian energies for the four dyes (less than 8 kJ/mol) suggested monolayer adsorption by exothermic, spontaneous, and physical reactions. The product demonstrated promising adsorption results even in the presence of other coexisting ions and showed significant recyclability properties.

4. EXPERIMENTAL WORK

4.1. Materials. The kaolinite mineral that was used in the scrolling process was obtained from CMRDI Institute, Egypt. The used chemicals are NaOH pellets (Sigma-Aldrich; 97% purity; CAS: 1310-73-2), dimethyl sulfoxide (DMSO) (Sigma-Aldrich; >99.5% purity; CAS: 67-68-5), methanol (Sigma-Aldrich; >99.9% purity; CAS: 67-56-1), and cetyltrimethylammonium bromide (CTAB) (Sigma-Aldrich; >98% purity; CAS: 57-09-0). The chemicals are of analytical grade and incorporated directly in the reactions without any purification processes. The safranin-O dye ($C_{20}H_{19}ClN_4$) (≥85% dye content, Sigma-Aldrich; CAS: 477-73-6), malachite green dye ($C_{23}H_{25}N_2$) (90% dye content, Sigma-Aldrich; CAS: 18015-76-4), Congo red dye ($C_{32}H_{22}N_6Na_2O_6S_2$) (34% dye content, Sigma-Aldrich; CAS: 573-58-0), and methyl orange dye ($C_{14}H_{14}N_3NaO_3S$) (85% dye content, Sigma-Aldrich; CAS: 547-58-0) powders were obtained from Sigma-Aldrich, Egypt, as the sources of the synthetic dye contaminants.

4.2. Synthesis Steps of KNTs. The production of KNTs was completed considering the three main steps reported by Abukhadra et al.[25] This involved breaking of the hydrogen bonds, exfoliation of the kaolinite layers, and scrolling of the exfoliated layers. About 15 g of the kaolinite powder was mixed with DMSO (50 mL; 80%), and the resulting mixture was stirred for about 24 h as an essential step to confirm the destruction of the hydrogen bonds and the intercalation of the kaolinite layers with the DMSO molecules. Afterward, the resulting particles from this stage were washed five times with methanol for nearly 20 min for developing hybrid materials of methanol-intercalated kaolinite known as methoxy kaolinite. This hybrid product was treated with the surfactant solution (500 mL of CTAB (1 mol/L)), and this continued for 2 days to verify effective expansion and exfoliation of the kaolinite layers from each other. The expansion step was continued effectively using sonication waves (80%) for another 48 h, which resulted finally in scrolled layers of kaolinite in the form of nanotubes. This was followed by separation of the product from the solution, which was washed with both methanol and distilled water and dried at 65 °C for 10 h.

4.3. Characterization Techniques. The crystal structure of KNTs was identified by a PANalytical X-ray diffractometer (Empyrean). The XRD results were obtained within a selected range from 5 to 70° and a scanning speed of 5°/min at 40 kV. A scanning electron microscope (Gemini, Zeiss-Ultra 55) was employed for determining the surficial morphology. The microscopic investigation was performed after coating the material using thin gold layers and at a certain voltage of 30 kV as an accelerating voltage. A transmission electron microscope (JEOL-JEM2100) was used for studying the internal structures of KNTs at 200 kV as an acceleration voltage. A Fourier transform infrared spectrometer (Shimadzu) was used to follow the expected changes in the chemical groups of KNTs. The spectrum of the material was determined at scans of 37°, adjusted resolution of about 4 cm^{-1}, and selected frequency from 400 cm^{-1} as the starting point to 4000 cm^{-1} as the upper limit. The porosity and the surface area of KNTs were measured based on its N_2 adsorption/desorption isotherm curve that was treated by BJH and Brunauer–Emmett–Teller (BET) methods. This was conducted using a surface area analyzer after a preprocessing step that involved degassing of the material for 5 h at 300 °C under vacuum, and the estimation temperature was adjusted to be 77 K. ζ potential values of the synthetic KNTs were determined at different pH values using a zetasizer with a disposable ζ cell (Malvern, version 7.11) to detect $pH_{(zpc)}$.

4.4. Adsorption System. The tested samples were prepared by directly dissolving certain quantities of the dye powder in distilled water (1000 mg/L in 1000 mL). The affinity of KNTs for SF, MG, CR, and MO dyes was evaluated by batch uptake experiments considering the main variables (pH, time (min), KNT dosage (g/L), tested dye concentration (mg/L), and temperature (°C)). All of the accomplished experiments for each variable were repeated as three runs, and the determined results were presented as average values during the evaluation of the uptake behavior. The principal procedures involved a homogeneous dispersion of the KNTs at a certain dosage (0.2–1 g/L) in 500 mL of dye aqueous solutions (50–400 mg/L) for certain intervals (30–480 min). As an initial stage, the influence of pH was examined from pH 2 as the starting point to pH 10 as the upper experimental limit. By the end of the experiments, the purified samples were analyzed directly by a UV–vis spectrophotometer to measure the residuals considering λ_{max} values of the dyes (521 nm for SF, 617 nm for MG, 497 nm for CR, and 460 nm for MO).

■ ASSOCIATED CONTENT

Supporting Information

The Supporting Information is available free of charge at https://pubs.acs.org/doi/10.1021/acsomega.0c05430.

Theoretical equations of the kinetic and isotherm models (Table S1); TEM image of kaolinite (Figure S1); N_2 adsorption/desorption isotherm curve of KNTs (Figure S2); uptake capacity of KNTs at different concentrations of the dyes (Figure S3); Elovich kinetic model (Figure S4); fitting of the results with the van't Hoff equation (Figure S5); recyclability results of KNTs (Figure S6); and FT-IR spectra of KNTs after the adsorption tests (Figure S7) (PDF)

https://dx.doi.org/10.1021/acsomega.0c05430
ACS Omega 2021, 6, 845–856

AUTHOR INFORMATION

Corresponding Authors

Mostafa R. Abukhadra − *Geology Department, Faculty of Science and Materials Technologies and Their Applications Lab, Geology Department, Faculty of Science, Beni-Suef University, Beni-Suef City 65211, Egypt*; orcid.org/0000-0001-5404-7996; Email: abukhadra89@science.bsu.edu.eg

Ahmed M. El-Sherbeeny − *Industrial Engineering Department, College of Engineering, King Saud University, Riyadh 11421, Saudi Arabia*; Email: aelsherbeeny@ksu.edu.sa

Authors

Merna Mostafa − *Geology Department, Faculty of Science and Materials Technologies and Their Applications Lab, Geology Department, Faculty of Science, Beni-Suef University, Beni-Suef City 65211, Egypt*

Mohammed A. El-Meligy − *Advanced Manufacturing Institute, King Saud University, Riyadh 11421, Saudi Arabia*

Ahmed Nadeem − *Department of Pharmacology & Toxicology, College of Pharmacy, King Saud University, Riyadh 12372, Saudi Arabia*

Complete contact information is available at: https://pubs.acs.org/10.1021/acsomega.0c05430

Author Contributions

This article was written through the contributions of all authors. All authors have given approval to the final version of the manuscript

Notes

The authors declare no competing financial interest.

ACKNOWLEDGMENTS

The authors extend their appreciation to the Deputyship for Research & Innovation, "Ministry of Education" in Saudi Arabia, for funding this research work through project number IFKSURG-1440-047.

REFERENCES

(1) Iqbal, M.; Abbas, M.; Nisar, J.; Nazir, A.; Qamar, A. Bioassays based on higher plants as excellent dosimeters for ecotoxicity monitoring: a review. *Chem. Int.* **2019**, *5*, 1−80.

(2) Bhat, S. A.; Zafar, F.; Mondal, A. H.; Mirza, A. U.; Haq, Q. M. R.; Nishat, N. Efficient removal of Congo red dye from aqueous solution by adsorbent films of polyvinyl alcohol/melamine-formaldehyde composite and bactericidal effects. *J. Cleaner Prod.* **2020**, *255*, No. 120062.

(3) Abbas, M.; Adil, M.; Ehtisham-ul-Haque, S.; Munir, B.; Yameen, M.; Ghaffar, A.; Shar, G. A.; Tahir, M. A.; Iqbal, M. *Vibrio fischeri* bioluminescence inhibition assay for ecotoxicity assessment: A review. *Sci. Total Environ.* **2018**, *626*, 1295−1309.

(4) Saad, A. M.; Abukhadra, M. R.; Ahmed, S. A. K.; Elzanaty, A. M.; Mady, A. H.; Betiha, M. A.; Shim, J. J.; Rabie, A. M. Photocatalytic degradation of malachite green dye using chitosan supported ZnO and Ce−ZnO nano-flowers under visible light. *J. Environ. Manage.* **2020**, *258*, No. 110043.

(5) Zafar, M. N.; Amjad, M.; Tabassum, M.; Ahmad, I.; Zubair, M. $SrFe_2O_4$ nanoferrites and $SrFe_2O_4$/ground eggshell nanocomposites: fast and efficient adsorbents for dyes removal. *J. Cleaner Prod.* **2018**, *199*, 983−994.

(6) Rahdar, S.; Rahdar, A.; Zafar, M. N.; Shafqat, S. S.; Ahmadi, S. Synthesis and characterization of MgO supported Fe−Co−Mn nanoparticles with exceptionally high adsorption capacity for rhodamine B dye. *J. Mater. Res. Technol.* **2019**, *8*, 3800−3810.

(7) Munir, M.; Nazar, M. F.; Zafar, M. N.; Zubair, M.; Ashfaq, M.; Hosseini-Bandegharaei, A.; Khan, S. U. D.; Ahmad, A. Effective Adsorptive Removal of Methylene Blue from Water by Didodecyldimethylammonium Bromide-Modified Brown Clay. *ACS Omega* **2020**, *5*, 16711−16721.

(8) Shaban, M.; Abukhadra, M. R.; Shahien, M. G.; Khan, A. A. P. Upgraded modified forms of bituminous coal for the removal of safranin-T dye from aqueous solution. *Environ. Sci. Pollut. Res.* **2017**, *24*, 18135−18151.

(9) Ghamkhari, A.; Mohamadi, L.; Kazemzadeh, S.; Zafar, M. N.; Rahdar, A.; Khaksefidi, R. Synthesis and characterization of poly(styrene-block-acrylic acid) diblock copolymer modified magnetite nanocomposite for efficient removal of penicillin G. *Composites, Part B* **2020**, *182*, No. 107643.

(10) Abukhadra, M. R.; Mohamed, A. S. Adsorption removal of safranin dye contaminants from water using various types of natural zeolite. *Silicon* **2019**, *11*, 1635−1647.

(11) Chen, H.; Liu, T.; Meng, Y.; Cheng, Y.; Lu, J.; Wang, H. Novel graphene oxide/aminated lignin aerogels for enhanced adsorption of malachite green in wastewater. *Colloids Surf., A* **2020**, *603*, No. 125281.

(12) Rabie, A. M.; Abukhadra, M. R.; Rady, A. M.; Ahmed, S. A.; Labena, A.; Mohamed, H. S.; Betiha, M. A.; Shim, J.-J. Instantaneous photocatalytic degradation of malachite green dye under visible light using novel green Co−ZnO/algae composites. *Res. Chem. Intermed.* **2020**, *46*, 1955−1973.

(13) Sharma, G.; Sharma, S.; Kumar, A.; Naushad, M.; Du, B.; Ahamad, T.; Ghfar, A. A.; Alqadami, A. A.; Stadler, F. J. Honeycomb structured activated carbon synthesized from *Pinus roxburghii* cone as effective bioadsorbent for toxic malachite green dye. *J. Water Process Eng.* **2019**, *32*, No. 100931.

(14) Shaban, M.; Sayed, M. I.; Shahien, M. G.; Abukhadra, M. R.; Ahmed, Z. M. Adsorption behavior of inorganic-and organic-modified kaolinite for Congo red dye from water, kinetic modeling, and equilibrium studies. *J. Sol−Gel Sci. Technol.* **2018**, *87*, 427−441.

(15) Zhang, H.; Ma, J.; Wang, F.; Chu, Y.; Yang, L.; Xia, M. Mechanism of carboxymethyl chitosan hybrid montmorillonite and adsorption of Pb (II) and Congo red by CMC-MMT organic-inorganic hybrid composite. *Int. J. Biol. Macromol.* **2020**, *149*, 1161−1169.

(16) Waheed, A.; Mansha, M.; Kazi, I. W.; Ullah, N. Synthesis of a novel 3, 5-diacrylamidobenzoic acid based hyper-cross-linked resin for the efficient adsorption of Congo Red and Rhodamine B. *J. Hazard. Mater.* **2019**, *369*, 528−538.

(17) Olusegun, S. J.; Mohallem, N. D. Comparative adsorption mechanism of doxycycline and Congo red using synthesized kaolinite supported $CoFe_2O_4$ nanoparticles. *Environ. Pollut.* **2020**, *260*, No. 114019.

(18) Riaz, Q.; Ahmed, M.; Zafar, M. N.; Zubair, M.; Nazar, M. F.; Sumrra, S. H.; Ahmad, I.; Hosseini-Bandegharaei, A. NiO nanoparticles for enhanced removal of methyl orange: equilibrium, kinetics, thermodynamic and desorption studies. *Int. J. Environ. Anal. Chem.* **2020**, 1−20.

(19) Wu, Y.; Su, M.; Chen, J.; Xu, Z.; Tang, J.; Chang, X.; Chen, D. Superior adsorption of methyl orange by h-MoS_2 microspheres: Isotherm, kinetics, and thermodynamic studies. *Dyes Pigm.* **2019**, *170*, No. 107591.

(20) Kausar, A.; Iqbal, M.; Javed, A.; Aftab, K.; Nazli, Z.i.-H.; Bhatti, H. N.; Nouren, S. Dyes adsorption using clay and modified clay: A review. *J. Mol. Liq.* **2018**, *256*, 395−407.

(21) Bhatti, H. N.; Safa, Y.; Yakout, S. M.; Shair, O. H.; Iqbal, M.; Nazir, A. Efficient removal of dyes using carboxymethyl cellulose/alginate/polyvinyl alcohol/rice husk composite: Adsorption/desorption, kinetics and recycling studies. *Int. J. Biol. Macromol.* **2020**, *150*, 861−870.

(22) Mohamed, F.; Abukhadra, M. R.; Shaban, M. Removal of safranin dye from water using polypyrrole nanofiber/Zn-Fe layered double hydroxide nanocomposite (Ppy NF/Zn-Fe LDH) of enhanced

adsorption and photocatalytic properties. *Sci. Total Environ.* **2018**, *640−641*, 352−363.
(23) Alaqarbeh, M. M.; Shammout, M. W.; Awwad, A. M. Nano platelets kaolinite for the adsorption of toxic metal ions in the environment. *Chem. Int.* **2020**, *6*, 49−55.
(24) Singh, R.; Dutta, S. The role of pH and nitrate concentration in the wet chemical growth of nano-rods shaped ZnO photocatalyst. *Nano-Struct. Nano-Objects* **2019**, *18*, No. 100250.
(25) Abukhadra, M. R.; Bakry, B. M.; Adlii, A.; Yakout, S. M.; El-Zaidy, M. E. Facile conversion of kaolinite into clay nanotubes (KNTs) of enhanced adsorption properties for toxic heavy metals (Zn^{2+}, Cd^{2+}, Pb^{2+}, and Cr^{6+}) from water. *J. Hazard. Mater.* **2019**, *374*, 296−308.
(26) Nausheen, S.; Bhatti, H. N.; Arif, K.; Nisar, J.; Iqbal, M. Native clay, $MnFe_2O_4$/clay composite and bio-composite efficiency for the removal of synthetic dye from synthetic solution: column versus batch adsorption studies. *Desalin. Water Treat.* **2020**, *187*, 219−231.
(27) Awwad, A.; Amer, M.; Al-aqarbeh, M. TiO_2-kaolinite nanocomposite prepared from the Jordanian Kaolin clay: Adsorption and thermodynamics of Pb (II) and Cd (II) ions in aqueous solution. *Chem. Int.* **2020**, *6*, 168−178.
(28) Abukhadra, M. R.; Allah, A. F. Synthesis and characterization of kaolinite nanotubes (KNTs) as a novel carrier for 5-fluorouracil of high encapsulation properties and controlled release. *Inorg. Chem. Commun.* **2019**, *103*, 30−36.
(29) Jiang, Y.; Abukhadra, M. R.; Refay, N. M.; Sharaf, M. F.; El-Meligy, M. A.; Awwad, E. M. Synthesis of chitosan/MCM-48 and *β*-cyclodextrin/MCM-48 composites as bio-adsorbents for environmental removal of Cd^{2+} ions; kinetic and equilibrium studies. *React. Funct. Polym.* **2018**, *54*, No. 104675.
(30) Shaban, M.; Abukhadra, M. R.; Mohamed, A. S.; Shahien, M. G.; Ibrahim, S. S. Synthesis of mesoporous graphite functionalized by nitrogen for efficient removal of safranin dye utilizing rice husk ash; equilibrium studies and response surface optimization. *J. Inorg. Organomet. Polym. Mater.* **2018**, *28*, 279−294.
(31) Purkait, M. K.; Maiti, A.; Dasgupta, S.; De, S. Removal of congo red using activated carbon and its regeneration. *J. Hazard. Mater.* **2007**, *145*, 287−295.
(32) El-Zeiny, H. M.; Abukhadra, M. R.; Sayed, O. M.; Osman, A. H. M.; Ahmed, S. Insight into novel *β*-cyclodextrin-grafted-poly (N-vinylcaprolactam) nanogel structures as advanced carriers for 5-fluorouracil: Equilibrium behavior and pharmacokinetic modeling. *Colloids Surf., A.* **2020**, *586*, No. 124197.
(33) Shaban, M.; Abukhadra, M. R.; Khan, A. A. P.; Jibali, B. M. Removal of Congo red, methylene blue and Cr (VI) ions from water using natural serpentine. *J. Taiwan Inst. Chem. Eng.* **2018**, *82*, 102−116.
(34) Abukhadra, M. R.; Adlii, A.; El-Sherbeeny, A. M.; Soliman, A.T.A.; Abd Elatty, E. Promoting the decontamination of different types of water pollutants (Cd^{2+}, safranin dye, and phosphate) using a novel structure of exfoliated bentonite admixed with cellulose nanofiber. *J. Environ. Manage.* **2020**, *273*, No. 111130.
(35) Tu, Y.; Feng, P.; Ren, Y.; Cao, Z.; Wang, R.; Xu, Z. Adsorption of ammonia nitrogen on lignite and its influence on coal water slurry preparation. *Fuel* **2019**, *238*, 34−43.
(36) Li, Z.; Wang, L.; Meng, J.; Liu, X.; Xu, J.; Wang, F.; Brookes, P. Zeolite-supported nanoscale zero-valent iron: New findings on simultaneous adsorption of Cd (II), Pb (II), and As (III) in aqueous solution and soil. *J. Hazard. Mater.* **2018**, *344*, 1−11.
(37) Sherlala, A. I. A.; Raman, A. A. A.; Bello, M. M.; Buthiyappan, A. Adsorption of arsenic using chitosan magnetic graphene oxide nanocomposite. *J. Environ. Manage.* **2019**, *246*, 547−556.
(38) Tran, H. N.; You, S.-J.; Hosseini-Bandegharaei, A.; Chao, H. P. Mistakes and inconsistencies regarding adsorption of contaminants from aqueous solutions: a critical review. *Water Res.* **2017**, *120*, 88−116.
(39) Akbour, R. A.; Ouachtak, H.; Jada, A.; Akhouairi, S.; Addi, A. A.; Douch, J.; Hamdani, M. Humic acid covered alumina as adsorbent for the removal of organic dye from coloured effluents. *Desalin. Water Treat.* **2018**, *112*, 207−217.
(40) Abukhadra, M. R.; Mostafa, M. Effective decontamination of phosphate and ammonium utilizing novel muscovite/phillipsite composite; equilibrium investigation and realistic application. *Sci. Total Environ.* **2019**, *667*, 101−111.
(41) Sahu, M. K.; Sahu, U. K.; Patel, R. K. Adsorption of safranin-O dye on CO_2 neutralized activated red mud waste: process modelling, analysis and optimization using statistical design. *RSC Adv.* **2015**, *5*, 42294−42304.
(42) Han, X.; Yuan, J.; Ma, X. Adsorption of malachite green from aqueous solutions onto lotus leaf: equilibrium, kinetic, and thermodynamic studies. *Desalin. Water Treat.* **2014**, *52*, 5563−5574.
(43) Umamaheswari, C.; Lakshmanan, A.; Nagarajan, N. S. Green synthesis, characterization and catalytic degradation studies of gold nanoparticles against congo red and methyl orange. *J. Photochem. Photobiol., B* **2018**, *178*, 33−39.
(44) Maged, A.; Kharbish, S.; Ismael, I. S.; Bhatnagar, A. Characterization of activated bentonite clay mineral and the mechanisms underlying its sorption for ciprofloxacin from aqueous solution. *Environ. Sci. Pollut. Res.* **2020**, *27*, 32980−32997.
(45) Abukhadra, M. R.; Adlii, A.; El-Sherbeeny, A. M.; Soliman, A. T. A.; Abd Elatty, E. Promoting the decontamination of different types of water pollutants (Cd^{2+}, safranin dye, and phosphate) using a novel structure of exfoliated bentonite admixed with cellulose nanofiber. *J. Environ. Manage.* **2020**, *273*, No. 111130.
(46) Abukhadra, M. R.; Shaban, M. Recycling of different solid wastes in synthesis of high-order mesoporous silica as adsorbent for safranin dye. *Int. J. Environ. Sci. Technol.* **2019**, *16*, 7573−7582.
(47) Kumar, K. V.; Sivanesan, S. Comparison of linear and non-linear method in estimating the sorption isotherm parameters for safranin onto activated carbon. *J. Hazard. Mater.* **2005**, *123*, 288−292.
(48) Kaur, S.; Rani, S.; Mahajan, R. K.; Asif, M.; Gupta, V. K. Synthesis and adsorption properties of mesoporous material for the removal of dye safranin: kinetics, equilibrium, and thermodynamics. *J. Ind. Eng. Chem.* **2015**, *22*, 19−27.
(49) Reddy, Y. S.; Magdalane, C. M.; Kaviyarasu, K.; Mola, G. T.; Kennedy, J.; Maaza, M. Equilibrium and kinetic studies of the adsorption of acid blue 9 and Safranin O from aqueous solutions by MgO decked FLG coated Fuller's earth. *J. Phys. Chem. Solids* **2018**, *123*, 43−51.
(50) Debnath, S.; Parashar, K.; Pillay, K. Ultrasound assisted adsorptive removal of hazardous dye Safranin O from aqueous solution using crosslinked graphene oxide-chitosan (GOCH) composite and optimization by response surface methodology (RSM) approach. *Carbohydr. Polym.* **2017**, *175*, 509−517.
(51) Abukhadra, M. R.; El-Meligy, M. A.; El-Sherbeeny, A. M. Evaluation and characterization of Egyptian ferruginous kaolinite as adsorbent and heterogeneous catalyst for effective removal of safranin-O cationic dye from water. *Arab. J. Geosci.* **2020**, *13*, No. 169.
(52) Fayazi, M.; Afzali, D.; Taher, M. A.; Mostafavi, A.; Gupta, V. K. Removal of Safranin dye from aqueous solution using magnetic mesoporous clay: optimization study. *J. Mol. Liq.* **2015**, *212*, 675−685.
(53) Arabkhani, P.; Asfaram, A. Development of a novel three-dimensional magnetic polymer aerogel as an efficient adsorbent for malachite green removal. *J. Hazard. Mater.* **2020**, *384*, No. 121394.
(54) Yildirim, A.; Bulut, Y. Adsorption behaviors of malachite green by using crosslinked chitosan/polyacrylic acid/bentonite composites with different ratios. *Environ. Technol. Innovation* **2020**, *17*, No. 100560.
(55) Zaidi, N. A. H. M.; Lim, L. B. L.; Usman, A. Enhancing adsorption of malachite green dye using base-modified *Artocarpus odoratissimus* leaves as adsorbents. *Environ. Technol. Innovation* **2019**, *13*, 211−223.
(56) Peighambardoust, S. J.; Bavil, O. A.; Foroutan, R.; Arsalani, N. Removal of malachite green using carboxymethyl cellulose-g-polyacrylamide/montmorillonite nanocomposite hydrogel. *Int. J. Biol. Macromol.* **2020**, *159*, 1122−1131.

https://dx.doi.org/10.1021/acsomega.0c05430
ACS Omega 2021, 6, 845−856

(57) Salamat, S.; Hadavifar, M.; Rezaei, H. Preparation of nanochitosan-STP from shrimp shell and its application in removing of malachite green from aqueous solutions. *J. Environ. Chem. Eng.* **2019**, *7*, No. 103328.
(58) Gao, M.; Wang, Z.; Yang, C.; Ning, J.; Zhou, Z.; Li, G. Novel magnetic graphene oxide decorated with persimmon tannins for efficient adsorption of malachite green from aqueous solutions. *Colloids Surf., A* **2019**, *566*, 48−57.
(59) Eltaweil, A. S.; Mohamed, H. A.; Abd El-Monaem, E. M.; El-Subruiti, G. M. Mesoporous magnetic biochar composite for enhanced adsorption of malachite green dye: Characterization, adsorption kinetics, thermodynamics and isotherms. *Adv. Powder Technol.* **2020**, *31*, 1253−1263.
(60) Raval, N. P.; Shah, P. U.; Shah, N. K. Malachite green "a cationic dye" and its removal from aqueous solution by adsorption. *Appl. Water Sci.* **2017**, *7*, 3407−3445.
(61) Gupta, K.; Khatri, O. P. Reduced graphene oxide as an effective adsorbent for removal of malachite green dye: plausible adsorption pathways. *J. Colloid Interface Sci.* **2017**, *501*, 11−21.
(62) Yu, M.; Han, Y.; Li, J.; Wang, L. CO_2-activated porous carbon derived from cattail biomass for removal of malachite green dye and application as supercapacitors. *Chem. Eng. J.* **2017**, *317*, 493−502.
(63) George, G.; Saravanakumar, M. P. Facile synthesis of carbon-coated layered double hydroxide and its comparative characterisation with Zn−Al LDH: application on crystal violet and malachite green dye adsorption-isotherm, kinetics and Box-Behnken design. *Environ. Sci. Pollut. Res.* **2018**, *25*, 30255−30256.
(64) Lei, C.; Pi, M.; Zhou, W.; Guo, Y.; Zhang, F.; Qin, J. Synthesis of hierarchical porous flower-like ZnO-AlOOH structures and their applications in adsorption of Congo Red. *Chem. Phys. Lett.* **2017**, *687*, 143−151.
(65) Nodehi, R.; Shayesteh, H.; Kelishami, A. R. Enhanced adsorption of congo red using cationic surfactant functionalized zeolite particles. *Microchem. J.* **2020**, *153*, No. 104281.
(66) Li, J.; Fan, Q.; Wu, Y.; Wang, X.; Chen, C.; Tang, Z.; Wang, X. Magnetic polydopamine decorated with Mg−Al LDH nanoflakes as a novel bio-based adsorbent for simultaneous removal of potentially toxic metals and anionic dyes. *J. Mater. Chem. A* **2016**, *4*, 1737−1746.
(67) Hu, H.; Liu, J.; Xu, Z.; Zhang, L.; Cheng, B.; Ho, W. Hierarchical porous Ni/Co-LDH hollow dodecahedron with excellent adsorption property for Congo red and Cr (VI) ions. *Appl. Surf. Sci.* **2019**, *478*, 981−990.
(68) Mohebali, S.; Bastani, D.; Shayesteh, H. Equilibrium, kinetic and thermodynamic studies of a low-cost biosorbent for the removal of Congo red dye: acid and CTAB-acid modified celery (*Apium graveolens*). *J. Mol. Struct.* **2019**, *1176*, 181−193.
(69) Lei, C.; Zhu, X.; Le, Y.; Zhu, B.; Yu, J.; Ho, W. Hierarchically porous NiO-Al_2O_3 nanocomposite with enhanced Congo red adsorption in water. *RSC Adv.* **2016**, *6*, 10272−10279.
(70) Liu, X.; Niu, C.; Zhen, X.; Wang, J.; Su, X. Novel approach for synthesis of boehmite nanostructures and their conversion to aluminum oxide nanostructures for remove Congo red. *J. Colloid Interface Sci.* **2015**, *452*, 116−125.
(71) Shaban, M.; Abukhadra, M. R.; Shahien, M. G.; Ibrahim, S. S. Novel bentonite/zeolite-NaP composite efficiently removes methylene blue and Congo red dyes. *Environ. Chem. Lett.* **2018**, *16*, 275−280.
(72) Chen, H.; Zheng, Y.; Cheng, B.; Yu, J.; Jiang, C. Chestnut husk-like nickel cobaltite hollow microspheres for the adsorption of Congo red. *J. Alloys Compd.* **2018**, *735*, 1041−1051.
(73) Zheng, Y.; Zhu, B.; Chen, H.; You, W.; Jiang, C.; Yu, J. Hierarchical flower-like nickel (II) oxide microspheres with high adsorption capacity of Congo red in water. *J. Colloid Interface Sci.* **2017**, *504*, 688−696.
(74) Zhang, L.; Liu, Q.; Hu, P.; Huang, R. Adsorptive removal of methyl orange using enhanced cross-linked chitosan/bentonite composite. *Desalin. Water Treat.* **2016**, *5736*, 17011−17022.
(75) Habiba, U.; Siddique, T. A.; Lee, J. J. L.; Joo, T. C.; Ang, B. C.; Afifi, A. M. Adsorption study of methyl orange by chitosan/polyvinyl alcohol/zeolite electrospun composite nanofibrous membrane. *Carbohydr. Polym.* **2018**, *191*, 79−85.
(76) Mahmoodian, H.; Moradi, O.; Shariatzadeha, B.; Salehf, T. A.; Tyagi, I.; Maity, A.; Asif, M.; Gupta, V. K. Enhanced removal of methyl orange from aqueous solutions by poly HEMA−chitosan-MWCNT nano-composite. *J. Mol. Liq.* **2015**, *202*, 189−198.
(77) Ahmad, A.; Razali, M. H.; Mamat, M.; Mehamod, F. S. B.; Amin, K. A. M. Adsorption of methyl orange by synthesized and functionalized-CNTs with 3-aminopropyltriethoxysilane loaded TiO_2 nanocomposites. *Chemosphere* **2017**, *168*, 474−482.
(78) Ibrahim, R. K.; El-Shafie, A.; Hin, L. S.; Mohd, N. S. B.; Aljumaily, M. M.; Ibraim, S.; AlSaadi, M. A. A clean approach for functionalized carbon nanotubes by deep eutectic solvents and their performance in the adsorption of methyl orange from aqueous solution. *J. Environ. Manage.* **2019**, *235*, 521−534.
(79) Amokrane, S.; Aid, A.; Nibou, D.; Trari, M. Adsorption of methyl orange on nanoparticles of a synthetic zeolite NaA/CuO. *C. R. Chim.* **2015**, *183*, 336−344.
(80) Lu, Y.; Jiang, B.; Fang, L.; Ling, F.; Gao, J.; Wu, F.; Zhang, X. High performance NiFe layered double hydroxide for methyl orange dye and Cr (VI) adsorption. *Chemosphere* **2016**, *152*, 415−422.
(81) Chen, Y.; Jing, C.; Zhang, X.; Jiang, D.; Liu, X.; Dong, B.; Feng, L.; Li, S.; Zhang, Y. Acid-salt treated CoAl layered double hydroxide nanosheets with enhanced adsorption capacity of methyl orange dye. *J. Colloid Interface Sci.* **2019**, *548*, 100−109.

https://dx.doi.org/10.1021/acsomega.0c05430
ACS Omega 2021, 6, 845−856